IOP Publishing Journal of Physics D: Applied Physics
J. Phys. D: Appl. Phys. **54** (2021) 335103 (8pp) https://doi.org/10.1088/1361-6463/abff7d

First-principles identification of deep energy levels of sulfur impurities in silicon and their carrier capture cross sections

Lele Cai[1], Shanshan Wang[1], Menglin Huang[1], Yu-Ning Wu[1,*] and Shiyou Chen[1,2,*]

[1] Key Laboratory of Polar Materials and Devices (MOE) and Department of Optoelectronics, East China Normal University, Shanghai 200241, People's Republic of China
[2] Collaborative Innovation Center of Extreme Optics, Shanxi University, Taiyuan, Shanxi 030006, People's Republic of China

E-mail: ynwu@phy.ecnu.edu.cn and chensy@ee.ecnu.edu.cn

Received 21 February 2021, revised 24 April 2021
Accepted for publication 10 May 2021
Published 4 June 2021

Abstract

Studies of the deep energy levels and nonradiative carrier capture induced by sulfur doping in silicon were initiated 60 years ago; however, the defect configurations, their deep energy levels, and the carrier capture cross sections are still not well understood. In this study, we focus on S_{Si} substitution, and perform a first-principles study of its defect configurations and the deep energy levels using hybrid exchange-correlation functional. We discover a new distortive configuration for S_{Si}^{+} besides the previously obtained structure with higher symmetry. For both S_{Si}^{+} configurations, the deep transition levels $\varepsilon(0/+)$ and $\varepsilon(+/2+)$ are determined as 0.35 eV and 0.68 eV below the conduction band minimum, respectively. As a benchmark calculation, the hole-capture cross sections for neutral and +1 charged states are obtained based on the distortive structure. The cross section for S_{Si}^{+} agrees with the experiment, demonstrating the multi-phonon process for S_{Si}^{+} capturing a hole, whereas the cross section of S_{Si}^{0} is significantly lower than the experimental data because hole capture by S_{Si}^{0} is an Auger-type process. Our calculations provide a benchmark for the evaluation of the cross section of carrier capture in semiconductors using multi-phonon nonradiative recombination theory.

Supplementary material for this article is available online

Keywords: nonradiative carrier capture, sulfur doping, first-principles study

(Some figures may appear in colour only in the online journal)

1. Introduction

Sulfur doping in silicon has not only been used to elevate the sensitivity of the photodiodes that detect photons with energies below the band gap of silicon [1, 2], but also to enhance the absorption of photons and improve the photoelectric efficiency of solar cells because of the induced deep energy levels [3, 4]. However, the conversion efficiency of sulfur-doped silicon solar cells is decided not only by the concentration of sulfur but also by the the defect configurations [5], because deep energy levels in solar cells also induce the nonradiative carrier recombination via the Shockley–Read–Hall process, which in turn reduces the photogenerated carrier densities as well as the carrier lifetime, and thus reduces the performance of photovoltaic semiconductors [6–8]. Therefore, an in-depth understanding of the defect configurations and carrier

* Authors to whom any correspondence should be addressed.

recombination effects introduced by sulfur doping is of great importance to improve photovoltaic conversion efficiency.

Nevertheless, sulfurdoping in silicon has been underresearched both experimentally and theoretically. The earliest experimental studies of sulfurdoping in silicon include the work done by Carlson *et al* [9], who found that sulfur acted as a donor impurity, and donor levels were E_c—0.18 eV and E_c—0.37 eV, respectively, where E_c is the conduction band minimum (CBM). Krag and Zeiger [10] performed optical characterization at a low temperature and determined four ground-state energies: 0.109 eV, 0.187 eV, 0.368 eV, and 0.612 eV below E_c, respectively. Subsequent experiments have further determined that the four main energy levels generated from sulfurdoping are 0.188 eV, 0.318 eV, 0.371 eV, and 0.614 eV below E_c, respectively. In addition, they suggested that the energy levels are probably mainly caused by two defects: isolated substitutional sulfur (S_S) and molecular substitutional sulfur (S_{2S}) [11–21]. However, disagreement about the specific values of the defect energy levels still exists depending on different experiments. In terms of the nonradiative carrier recombination, Kleverman *et al* [17] employed a deep-level transient spectroscopy technique and a pulse-train method to measure the values of hole-capture cross section of single ionized S^+, and also assessed that the process of hole capture may be a multi-phonon nonradiative emission process or a combination of multi-phonon nonradiative emission and radiative capture process. From a theoretical perspective, Mo *et al* [22] found that, for an isolated S-atom in silicon, the lowest energy configuration is the substitution site by first-principles calculations. Based on the substitution defect type, Coutinho *et al* [23] calculated the transition energy levels of S-related defects in Si using a formation energy method and a marker method, but the results of these methods disagree. The formation energy method does not give transition energy levels that match the experiments for S_S and S_{2S}, whereas the marker method can only obtain the energy level of S_{2S} that matches the experiment using the measured S_S energy level as a reference. Although the defect configuration was investigated in these studies, theoretical understanding of the carrier capture cross section has not yet been reported.

Analytical models and computational approaches for capture cross sections were developed from the 1950s [24–28]; based on this, the multi-phonon nonradiative recombination process in semiconductors has been extensively studied. In recent years, theoretical studies based on multiple computational methods for a nonradiative recombination process have mainly focused on direct band gap semiconductors, such as GaN [29–33], GaP [26, 30], CdTe [34], Cu_2ZnSnS_4 [35–37], and $Cu_2ZnSnSe_4$ [38], while studies on indirect semiconductor materials such as Si have rarely been reported [39]. In particular, a combination of an electron–phonon coupling effect and static coupling formalism is used to calculate the carrier capture cross section, while the electron–phonon coupling matrix elements can be obtained using the conventional finite difference method. For large systems, the conventional finite difference method has been prohibitively time-consuming, until Shi and Wang [29] and Shi *et al* [30] developed the variational method, which has been successfully utilized to study GaN and GaP. Subsequently, this has allowed quantitative evaluation of the capture cross section of deep energy levels in a large system [40].

In this paper, we conduct a first-principles study of the defect configurations and corresponding energy levels introduced by sulfur doping in Si, as well as the hole-capture cross sections of the deep energy levels. As a benchmark study for the indirect band gap materials, which is Si in our case, we utilize the static coupling theory and first-principles calculation of electron–phonon coupling matrix elements to calculate the hole-capture cross sections. Our main results mainly include the following three aspects. First, using the hybrid exchange-correlation functional, we determine the defect configurations of the S_{Si} substitution with different charged states, together with their corresponding deep energy levels. Other than the highly symmetric structure found in previous studies, a new distortive structure of S_{Si} substitution in a $+1$ charged state is discovered. Moreover, we obtain the hole-capture cross sections for a neutral and a $+1$ charged state, and the hole-capture cross section for $S_{Si}{}^+$ to $S_{Si}{}^{2+}$ agrees with the experiment. In addition, the highly symmetric structure of the $S_{Si}{}^+$ gives negligibly low hole-capture cross sections, so there is a low possibility of it getting involved in the hole-capture process.

2. Computational methods

2.1. Defect calculations

Our first-principles defect calculations are performed based on density-functional theory (DFT) [41, 42] as implemented in the Vienna *Ab initio* Simulation Package (VASP) [43, 44]. The ion–electron interaction is modeled by the frozen-core projector augmented wave method [45]. The Heyd-Scuseria-Ernzerhof (HSE06) [46] hybrid functional and spin-polarization are employed for all calculations, in which 25% of the exact exchange is used. A 350 eV energy cutoff is adopted for the defect calculations. The defect is simulated using a 512-atom Si supercell with one Si atom substituted by a S atom. Only Γ point (0,0,0) is used to sample the first Brillouin zone. We test the defect formation energy depending on the size of the supercells, and find that a 512-atom Si supercell with Γ point is sufficient for the formation energy calculation. The lattice parameters are fixed and the internal coordinates are fully relaxed when the energy and force become smaller than 1×10^{-5} eV/atom and 0.01 eV Å^{-1}, respectively.

To calculate the transition energy levels of a defect, the formation energy of a defect is given by [47–49]:

$$\Delta H(\alpha, q) = E(\alpha, q) - E(\text{host}) + \sum_i n_i(\mu_i + E_i) + q(E_F + E_{VBM}(\text{host}) + \Delta V) + \Delta E_{MP}, \quad (1)$$

where μ_i is the chemical potential of element i, with reference to the total energy E_i of their elemental monomeric phases. The Fermi energy level E_F is referenced to the valence-band maximum (VBM) of the host of Si, so the value of E_F can vary between the VBM and the CBM. $E(\alpha, q)$ is the total

energy of the supercell with a defect in charged state q. E (host) and E_{VBM} (host) are the total energy and the eigenvalue of the VBM of the perfect silicon supercell, respectively. n_i is the number of atoms exchanged with the external environment during the formation of defects. ΔV is the potential alignment correction referenced to the core energy level of the atom far from the defect. Due to the periodic boundary conditions, the Coulomb interactions among the charged defects in repeating supercells are treated by the Makov–Payne correction ΔE_{MP}, as proposed by Lany and Zunger [49]. ΔE_{MP} is given by:

$$\Delta E_{\mathrm{MP}} = (1+f)\frac{\alpha \times q^2}{2\varepsilon L} \tag{2}$$

where $\alpha = 1.4186$ is the Madelung constant and $\varepsilon = 11.9$ is the relative dielectric constant. $L = 21.72$ Å and $1+f \approx \frac{2}{3}$ are applied for all defect calculations.

The defect transition energy level $\varepsilon(q/q')$ is defined as the Fermi energy level at which a defect transits from a q-charged state to a q'-charged state. The defect transition energy level relative to the VBM is given by:

$$\varepsilon(q/q') = \frac{\Delta H(\alpha, q) - \Delta H(\alpha, q')}{q - q'}. \tag{3}$$

2.2. Hole-capture cross section

The variational method proposed by Shi and Wang [29] is adopted to calculate the electron–phonon coupling matrix elements. This method only requires two self-consistent field calculations, which is significantly faster than the traditional finite-difference method. The form of electron–phonon coupling matrix elements is given by:

$$\left\langle \varphi_f \left| \frac{\partial H}{\partial Q_k} \right| \varphi_i \right\rangle = \sum_R \frac{\mu_k(R)}{\sqrt{M_R}} \left\langle \varphi_f \left| \frac{\partial H}{\partial R} \right| \varphi_i \right\rangle, \tag{4}$$

where f and i denote the final and initial states. M_R is the mass of the Rth atom and $\mu_k(R)$ is the Rth component of the Kth phonon eigenvector. Because of the large 512-atom supercell, the Perdew–Burke–Ernzerhof (PBE) [50] functional and spin-polarization are employed for the calculation of phonon modes using the finite displacement method, as implemented in the VASP code. The single-particle Hamiltonian H is given by:

$$H = -\frac{\hbar^2}{2}\sum_k \nabla^2 + V_{\mathrm{tot}} + \sum_{L,R} |\phi_{L,R}\rangle\langle\phi_{L,R}|, \tag{5}$$

where V_{tot} is the total local potential for a given atomic configuration and $|\phi_{L,R}\rangle$ is the non-local potential projector for atom R and angular momentum L. By plugging equations (5) to (4), the electron–phonon coupling constant is given by:

$$\left\langle \varphi_f \left| \frac{\partial H}{\partial R} \right| \varphi_i \right\rangle = \left\langle \varphi_f \left| \frac{\partial V_{tot}}{\partial R} \right| \varphi_i \right\rangle \sum_{L,R} \times \left\langle \varphi_f \left| \frac{\partial}{\partial R} \left(|\phi_{L,R}\rangle \langle \phi_{L,R}| \right) \right| \varphi_i \right\rangle. \tag{6}$$

The first term on the right-hand side is evaluated by $\left\langle \varphi_f \left| \frac{\partial V_{\mathrm{tot}}}{\partial R} \right| \varphi_i \right\rangle = \int \rho_{fi} \frac{\partial V_{\mathrm{tot}}}{\partial R} \mathrm{d}r = \frac{\mathrm{d}F_R}{\mathrm{d}\lambda}$, where $\rho_{fi} = \mathrm{Re}\left[\varphi_f^*(r)\varphi_i(r)\right]$ [29], and $\frac{\mathrm{d}F_R}{\mathrm{d}\lambda}$ is the change of the atomic forces introduced by a small variation in the charge density based on ρ_{fi}, or $\rho_\lambda(r) = \sum_k |\psi_k(r)|^2 + \lambda\rho_{fiS}$, where λ is chosen as 0.05 in our calculations. The second term is the non-local contribution, which can be calculated by the Hellman–Feynman theory in the conventional DFT calculations [51, 52]. For the spin-polarized case, when the defect captures a spin-up or spin-down electron, we add the variational charge density $\lambda\rho_{fi}$ to the charge density of the corresponding spin state. Capturing a hole is treated in the same way as capturing an electron. The calculations of electron–phonon coupling matrix elements are implemented in Quantum Espresso code [51].

The probability of nonradiative decay between electron state i or f is given by the static coupling theory [30, 35, 53, 54] as:

$$W_{\mathrm{if}} = \frac{2\pi}{\hbar}\sum_n\sum_m \rho(i,n)\left|\sum\langle\psi_{\mathrm{f}}\left|\frac{\partial H}{\partial Q_k}\right|\psi_{\mathrm{i}}\rangle\langle\phi_{\mathrm{f},m}|Q_k|\phi_{\mathrm{i},n}\rangle\right|^2 \times \delta(\hbar\omega_{\mathrm{f}m} - \hbar\omega_{in} + \Delta E_{\mathrm{if}}), \tag{7}$$

where n, m, and k represent the initial phonon state, final phonon state, and phonon number, respectively. $\psi_f\left|\frac{\partial H}{\partial Q_k}\right|\psi_i$, also denoted as $|C_{\mathrm{if}}|$, are the calculated electron–phonon coupling matrix elements. $p(i,n)$ is the probability of the system being in the initial phonon state n. $\phi_{\mathrm{f},m}|Q_k|\phi_{\mathrm{i},n}$ are the lattice transition matrix elements between the initial and final phonon states, and $\boldsymbol{Q}_k$ is the coordiante of the kth phonon. $\hbar w_{\mathrm{f}m}$ and $\hbar\omega_{in}$ are the energy of the initial and final state phonons, respectively. ΔE_{if} is the energy difference between the initial and final states. All parameters are obtained using spin-polarized calculations.

Based on the nonradiative decay probability W_{if}, the carrier capture rate B is calculated as $B = S(T) \times V \times W_{\mathrm{if}}$, where $S(T)$ is the Sommerfeld factor [36, 55, 56], which characterizes the Coulomb interaction between carriers and defects at temperature T. V is the volume of the supercell. In our work, we study the process of hole capture by the donor level, so the Sommerfeld factor $S(T)$ denotes the repulsive interaction between a defect in charged state Q and a carrier with charge q, and is given by:

$$S(T) = \frac{8}{\sqrt{3}}\left(\frac{\pi^2 Q^2 m_{\mathrm{h}}^* q^2}{2\hbar^2\varepsilon^2 k_{\mathrm{B}}T}\right)^{\frac{2}{3}} \exp\left[-3\left(\frac{\pi^2 Q^2 m_{\mathrm{h}}^* q^2}{2\hbar^2\varepsilon^2 k_{\mathrm{B}}T}\right)^{\frac{1}{3}}\right], \tag{8}$$

where $m_{\mathrm{h}}^* = 0.7m_0$ is the effective mass of the hole and ε is the dielectric constant of crystalline silicon. k_{B} is the Boltzmann constant. With the hole-capture rate B_{h} calculated, the corresponding hole-capture cross section is calculated as $\sigma_{\mathrm{h}} = \frac{B_{\mathrm{h}}}{v_{\mathrm{h}}}$, where $v_{\mathrm{h}} = \sqrt{\frac{3k_{\mathrm{B}}T}{m_{\mathrm{h}}^*}}$ is the thermal velocity of the hole.

3. Results and discussion

The band gap of the 512-atom Si supercell at Γ point is calculated as 1.2 eV, which is almost identical to the result of the primitive cell, 1.15 eV. The detailed band structure of the 512-atom Si supercell is described in the supplementary information (available online at stacks.iop.org/JPD/54/335103/mmedia). As mentioned above, the sulfur atom is found to prefer replacing the silicon atom when an isolated sulfur atom is doped into crystalline silicon [22]. Therefore, we focus on the S_{Si} substitution. Taking spin-polarization into consideration, we optimize the structures of the 0, +1, and +2 (three charged states of the S_{Si} substitution) separately and calculate their total energies. Based on our calculations, the S_{Si} substitution is revealed as a donor defect that can be stabilized at three charged states: 0, +1, and +2.

As shown in figures 1(a) and (c), the sulfur atom is found to be centrally located in the middle of four surrounding Si atoms in S_{Si}^{0} and S_{Si}^{2+} substitutions. The S–Si bond lengths in S_{Si}^{0} and S_{Si}^{2+} substitutions are 2.45 Å and 2.42 Å, respectively. The shortening of the S–Si bond length in S_{Si}^{2+} is mainly due to a stronger Coulomb interaction between the defect center S_{Si}^{2+} and the surrounding electrons. Interestingly, two distinct stable structures for S_{Si}^{+} substitution, denoted as S_{Si}^{+}-A and S_{Si}^{+}-B (figures 1(b) and (d)), are obtained after the structure optimization. Similar to the structure of S_{Si}^{2+} substitution, the S_{Si}^{+}-A has four equivalent S–Si bonds around the S atom, with the same bond lengths 2.44 Å, as shown in figure 1(b). Due to the weaker Coulomb interaction than S_{Si}^{2+} substitution, the S–Si bond length in S_{Si}^{+}-A is slightly longer. S_{Si}^{+}-B exhibits a much more distortive structure with symmetry breaking, which is similar to the distortive structure of the Mg_{Ga} defect found in GaN [57]. As shown in figure 1(d), S_{Si}^{+}-B has three short S–Si bonds (2.33 Å) and one long bond (2.86 Å). Such a distortive structure is not observed in either previous Perdew -Wang 91 (PW91) [23] or our PBE calculations. The total energy of the S_{Si}^{+}-B structure is calculated to be 0.003 eV lower than that of the S_{Si}^{+}-A structure.

In figures 1(e) and (f), we also plot the charge densities of the defect states of S_{Si}^{+}-A and S_{Si}^{+}-B. The defect states for S_{Si}^{+}-A and S_{Si}^{+}-B are both the antibonding states of s-p hybridization of the S–Si bonds; however, the defect state for S_{Si}^{+}-A is contributed to by all four S–Si bonds around S, while the defect state for S_{Si}^{+}-B is mainly localized on the longest S–Si bond. Using the climbing image nudged elastic band method [58], we find that the energy barrier for the structure transition from the S_{Si}^{+}-B to S_{Si}^{+}-A is 0.01 eV.

Figure 2(a) shows the relative formation energies of the three charged states of the S_{Si} substitution calculated using the method as described in equation (1). Although S_{Si}^{+} has two different structures, their total energies are almost the same and the calculated formation energies and transition energy levels are almost identical. Therefore, we only plot the result of the spin-polarization of a S_{Si}^{+}-B in figure 2(a). The calculated $\varepsilon(0/+)$ and $\varepsilon(+/2+)$ levels are 0.349 eV and 0.678 eV below the CBM, which are deep energy levels in the Si gap. Our results accurately agree with the experimental values; i.e. E_c—0.32 eV and E_c—0.61 eV, respectively [13–15, 17]. As a comparison, the study by Coutinho *et al* [23] determines the transition energy levels at 0.78 eV and 1.25 eV below the CBM, respectively. Such a discrepancy is possibly due to the correction from the HSE06 hybrid functional. It is also essential to perform spin-polarized calculations, because non-spin-polarized calculations provide the wrong $\varepsilon(0/+)$ and $\varepsilon(+/2+)$ levels at 0.408 eV and 0.619 eV below the CBM. Therefore, it is also necessary to use spin-polarized calculations for the following study of the hole-capture cross section.

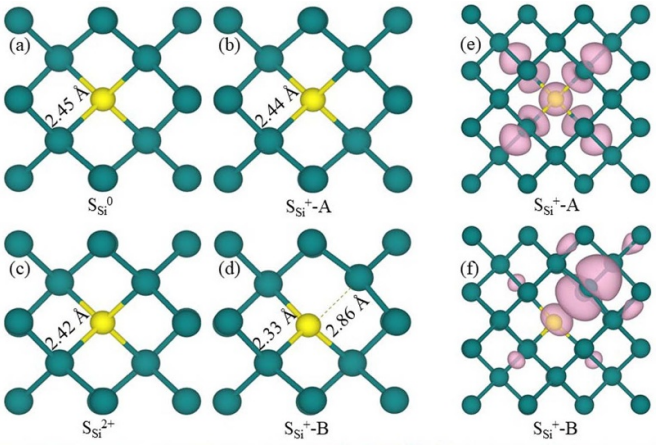

Figure 1. The atomic structures of S_{Si} substitution in three charged states: (a) S_{Si}^{+0}, (b) S_{Si}^{+}-A, (c) S_{Si}^{2+}, and (d) S_{Si}^{+}-B. The charge densities of the defect states of (e) S_{Si}^{+}-A and (f) S_{Si}^{+}-B. S atom and Si atom are shown in yellow and green, respectively.

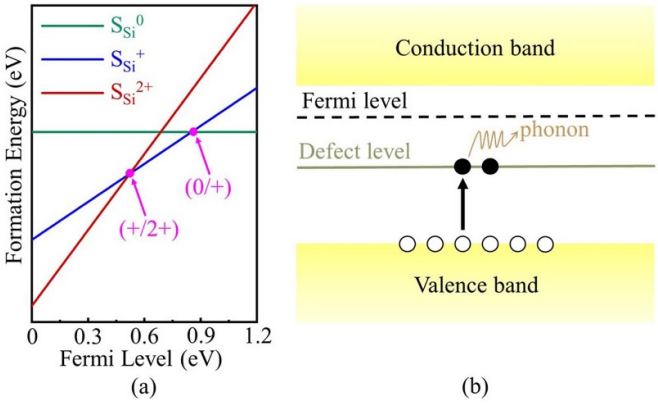

Figure 2. (a) HSE06 calculated the relative formation energies of the S_{Si} substitution at different charged states as functions of the Fermi level, using spin-polarized calculations. (b) Multi-phonon nonradiative recombination process in n-type Si.

Experimentally, S can be doped into both n-type and p-type Si to form defects and generates deep energy levels that introduce the nonradiative recombination [2, 4, 19, 21]. Figure 2(b) shows a schematic diagram of the nonradiative recombination process for S doping in n-type silicon. In n-type Si samples, the Fermi energy level is close to the conduction band, and the deep energy level is usually occupied with electrons carriers. The deep energy level can capture a hole from the VBM, leading to a transition from the neutral state to the +1 charged

state, the cross section of which is denoted as σ_{S^0}. It is also possible that a second hole is captured from the VBM, leading to a transition from the +1 charged state to the +2 charged state, the cross section of which is denoted as σ_{S^+}. Due to the high concentration of electrons in n-type Si, the defect state easily captures an electron from the CBM when the deep energy level is half occupied by electrons or empty. As a result, the hole-capture cross section plays a decisive role in this recombination. Carrier capture processes in p-type Si can be understood similarly by replacing holes with electrons [40].

Following equation (7), σ_{S^0} and σ_{S^+} as functions of temperature are calculated, as shown in figure 3. For σ_{S^0}, the initial and final states are $S_{Si}{}^0$ and $S_{Si}{}^+$, respectively, whereas for σ_{S^+}, the initial and final states are $S_{Si}{}^+$ and $S_{Si}{}^{2+}$, respectively. The phonon modes of the initial states are used to calculate electron–phonon coupling matrices during both hole-capture processes. Only the ground state structure of the +1 state $S_{Si}{}^+$-B is considered in the process of $S_{Si}{}^0$ to $S_{Si}{}^+$-B and $S_{Si}{}^+$-B to $S_{Si}{}^{2+}$. Cross sections for the process of $S_{Si}{}^0$ to $S_{Si}{}^+$-A and $S_{Si}{}^+$-A to $S_{Si}{}^{2+}$ are ignored, which will be discussed later. Since VBM is triply degenerated, we denote the three degenerate states as VBM_1, VBM_2, and VBM_3, separately from which $S_{Si}{}^0$ and $S_{Si}{}^+$ can possibly capture a hole. For all three degenerate VBM states, σ_{S^0} values are almost identical, and they increase as the temperature increases. The hole-capture cross sections of three VBM states are averaged following Matthiessen's rule, or $\frac{1}{\tau} = \frac{1}{\tau_1} + \frac{1}{\tau_2} + \frac{1}{\tau_3}$, and $\frac{1}{\tau_h} = \sigma \times v_h \times N_D$, where τ_h is the maximum lifetime of a hole carrier, N_D is the defect concentration, and v_h is the thermal velocity of the hole. Based on the structures of $S_{Si}{}^0$ to $S_{Si}{}^+$-B (figures 1(a) and (d)), the averaged σ_{S^0} is calculated to be within the range from 6.84×10^{-26} cm^2 to 1.66×10^{-22} cm^2 for the temperature range (100 K to 300 K). It is about six orders of magnitude lower than the experimental result [17] of 10^{-16} cm^2 at a temperature of 300 K. Such a discrepancy is possibly because the hole capture measured in the experiment is an Auger-type capture process [17], whereas our simulation of the capture process is based on the multi-phonon nonradiative recombination model. Similar to σ_{S^0}, based on the structures of $S_{Si}{}^+$-B to $S_{Si}{}^{2+}$ (figures 1(d) and (c)), the cross section σ_{S^+} also increases as the temperature increases; however, the VBM_1 state exhibits around 3.7 times higher values than VBM_2 and VBM_3. The average cross section σ_{S^+} is determined to be within the range from 1.44×10^{-24} cm^2 to 1.17×10^{-21} cm^2, which agrees well with the experimental result of about 10^{-23}–10^{-20} cm^2, as shown in figure 3. The calculated hole-capture cross section being lower than the experimental value by about an order of magnitude is probably due to the error induced by other co-existing defects in experimental samples, such as V_{Si}, i_S, etc. Although their concentration is low, they can still introduce errors in the hole-capture cross section. Another possible source of the difference is the approximations taken in our theory, such as the supercell approximation or static approximation [53, 54]. In fact, one order of magnitude difference is normally considered as reasonable agreement in calculations of carrier capture cross sections [33]. Therefore, such an agreement indicates that hole capture by $S_{Si}{}^+$-B is a multi-phonon nonradiative recombination process.

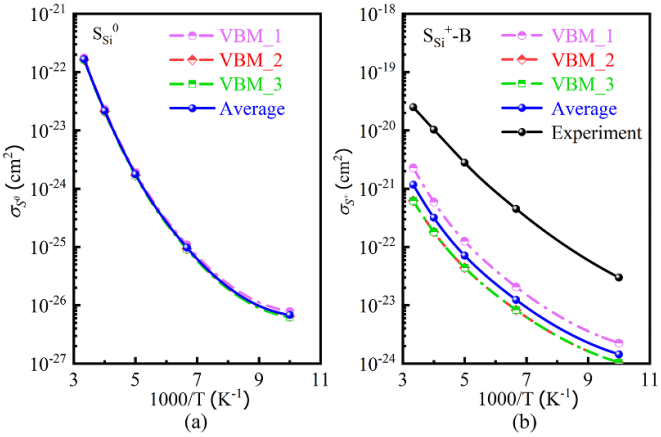

Figure 3. The hole-capture cross sections of the defect level which captures a hole from VBM_1, VBM_2, and VBM_3 separately as functions of the temperature. The average hole-capture cross sections of (a) $S_{Si}{}^0$ and (b) $S_{Si}{}^+$-B and the experimental values are shown in blue and black, respectively.

To reveal the contribution of the triplet states to the hole-capture cross section and the contribution of phonons in the hole-capture process, we plot the squared norms of electron–phonon coupling matrix elements $|C_{if}|^2$ as functions of phonon frequency (as shown in figure 4) to quantitatively analyze the contribution from each phonon during the capture of a hole. Figures 4(a)–(c) are the electron–phonon coupling matrix elements for $S_{Si}{}^0$ capturing a hole from VBM_1, VBM_2, and VBM_3, respectively. The phonons with the greatest electron–phonon coupling strength, which are located at around 4.2, 12.2, and 13.7 THz, show a large portion of resemblance, leading to the almost identical σ_{S^0} curves for the three VBM degenerate states in figure 3(a). For $S_{Si}{}^+$ capturing a hole, the coupling matrix elements of VBM_1 are generally greater than those of VBM_2 and VBM_3, especially in the low-frequency phonon part (figures 4(d)–(f)). As a result, $S_{Si}{}^+$ capturing a hole from VBM_1 is expected to have a larger hole-capture cross section than the other two. Such behavior is also consistent with the observed phenomenon that higher hole capture tends to be accompanied by more low frequency phonons [34].

Both σ_{S^0} and σ_{S^+} are significantly lower than the hole-capture cross section in Au-doped in Si (1.0×10^{-15} cm^2 at 300 K) measured by Bemski [59] and that of Pb_I antisite in $CH_3NH_3PbI_3$ (1.8×10^{-14} cm^2 at 300 K) predicted by Li *et al* [40]. Low σ_{S^0} is caused by the large energy difference between transition energy level $\varepsilon(0/+)$ and the VBM, and capturing the hole is not inherently easy. Low σ_{S^+} can be understood by the Coulomb repulsion between the $S_{Si}{}^+$ substitution and the already-existing hole in VBM.

To further illustrate why σ_{S^0} and σ_{S^+} are low, we plot the schematic diagram of configuration coordinates for (0/+) and (+/2+) transitions, as shown in figure 5. During the hole-capture process, a transition in the electronic state leads to a change in the equilibrium structure, as presented by the initial

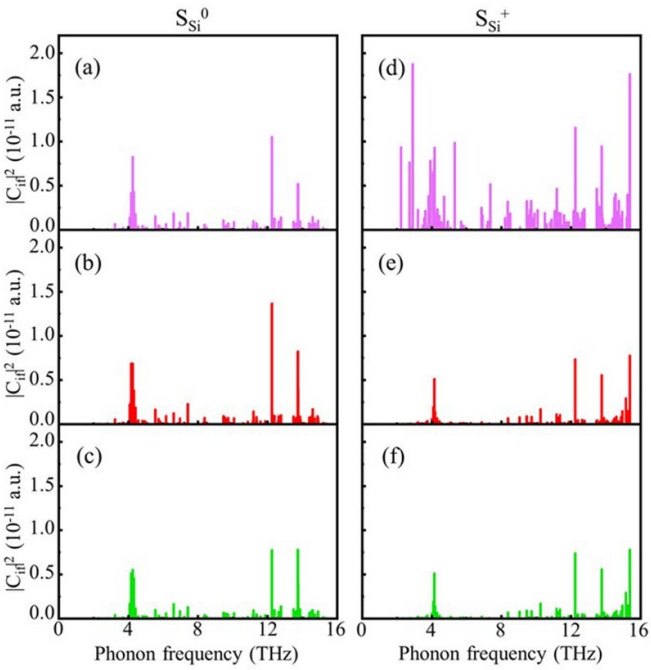

Figure 4. The squared norms of electron–phonon coupling matrix elements $|C_{if}|^2$ as functions of phonon frequency between the triplet states and defect state.

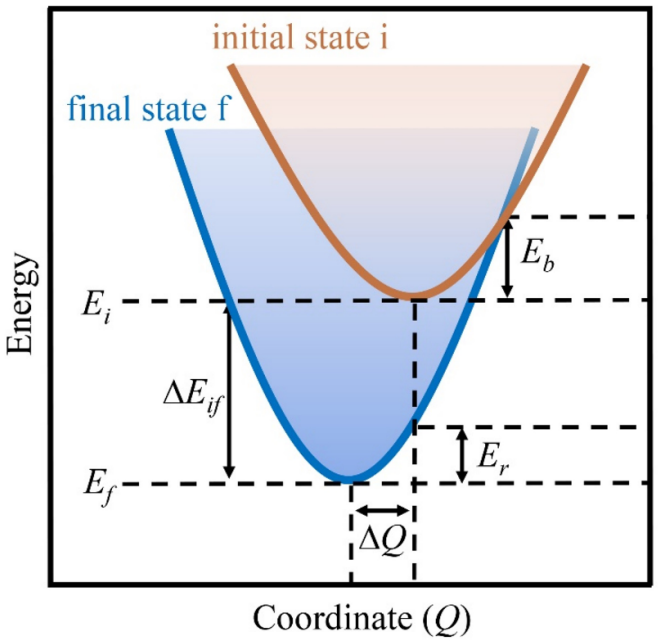

Figure 5. Schematic diagram of configuration coordinates for S_{Si} (i/f), such as (0/+) or (+/2+). Q is a relative configuration coordinate between the two charged states.

and final state curves with different equilibrium positions. The probability of the electronic state transition in equation (7) can be fitted following $W_{if} = C_1 + C_2 \exp\left[-\frac{E_b}{K_B T}\right]$ [31], where E_b is the energy barrier to be overcome when the initial state captures a hole and transforms to the final state. The energy barrier E_b can be calculated from $E_b = \frac{(\Delta E_{if} - E_r)^2}{4E_r}$ [35, 60], where $\Delta E_{if} = E_i - E_f$ is the transition energy level with E_i and E_f being the ground state energies of the initial and final states. E_r is the recombination energy produced during the structural relaxation from initial state towards the final state, and it can be calculated using $E_r = \frac{1}{2}\sum_k \omega_k{}^2 \Delta Q_k{}^2$, where ω_k is the frequency of phonon modes and ΔQ_k is the coordinate difference between the initial state and final state [26, 60]. As shown in table 1, the calculated recombination energy E_r for $S_{Si}{}^0$ capturing a hole is 0.195 eV, and the transition energy level ΔE_{if} is 0.851 eV above the VBM. The energy barrier E_b determined by E_r and ΔE_{if} is 0.552 eV. The E_r, ΔE_{if}, and E_b for $S_{Si}{}^+$ capturing a hole are 0.101 eV, 0.522 eV (above the VBM), and 0.439 eV, respectively. Compared to the 0.01 eV E_b and the corresponding 1.8×10^{-14} cm^2 hole-capture cross section of Pb_I antisite in $CH_3NH_3PbI_3$ [40], our calculated energy level barriers are much higher and therefore the capture cross sections are much lower. The E_b for $S_{Si}{}^+$ capturing a hole is lower by 0.114 eV than that for $S_{Si}{}^0$ capturing a hole, which is consistent with the σ_{S^+} being larger than the σ_{S^0}.

We also consider the hole-capture cross sections for the $S_{Si}{}^0$ to $S_{Si}{}^+$-A and $S_{Si}{}^+$-A to $S_{Si}{}^{2+}$ processes. Although the calculated transition energy levels of $S_{Si}{}^+$-A are almost the same as those based on structure $S_{Si}{}^+$-B, the hole-capture cross sections of the hole-capture processes through $S_{Si}{}^+$-A are found to be too low and beyond the numerical accuracy of our method. As shown in table 1, the energy barrier E_b for $S_{Si}{}^0$ to $S_{Si}{}^+$-A (11.537 eV) is much higher than $S_{Si}{}^0$ to $S_{Si}{}^+$-B (0.552 eV). This is mainly because the calculated recombination energy E_r for $S_{Si}{}^0$ to $S_{Si}{}^+$-A is 0.015 eV, which is an order of magnitude lower than that for $S_{Si}{}^0$ to $S_{Si}{}^+$-B (0.195 eV). Similarly, the E_b for $S_{Si}{}^+$-A to $S_{Si}{}^{2+}$ (2.625 eV) is much higher than that for $S_{Si}{}^+$-B to $S_{Si}{}^{2+}$ (0.439 eV). This is also attributed to the fact that the E_r for $S_{Si}{}^+$-A to $S_{Si}{}^{2+}$ (0.024 eV) is much lower than that for $S_{Si}{}^+$-A to $S_{Si}{}^{2+}$ (0.101 eV). Therefore, if hole-capture processes happen through the $S_{Si}{}^+$-A structure, it has to overcome a significantly higher energy barrier than through $S_{Si}{}^+$-B, and the corresponding cross sections for $S_{Si}{}^+$-A should be negligibly low compared to $S_{Si}{}^+$-B. The much higher energy barrier for $S_{Si}{}^+$-A can be attributed to its much smaller ΔQ, which is caused by the tiny structural differences between $S_{Si}{}^+$-A and $S_{Si}{}^0$/$S_{Si}{}^{2+}$. For a small ΔQ, the minimum curves of initial and final states in figure 5 nearly coincide at the same coordinates, so the recombination energy E_r becomes low, and the energy barrier E_b becomes high.

Table 1. Transition energy ΔE_{if} (relative to the VBM level), reorganization energy E_r, and transition energy barriers E_b for the $S_{Si}{}^0$ to $S_{Si}{}^+$-B, $S_{Si}{}^+$-B to $S_{Si}{}^{2+}$, $S_{Si}{}^0$ to $S_{Si}{}^+$-A, and $S_{Si}{}^+$-A to $S_{Si}{}^{2+}$ processes.

Structural transition	ΔE_{if} (eV)	E_r (eV)	E_b (eV)
$S_{Si}{}^0$ to $S_{Si}{}^+$-B	0.851	0.195	0.552
$S_{Si}{}^+$-B to $S_{Si}{}^{2+}$	0.522	0.101	0.439
$S_{Si}{}^0$ to $S_{Si}{}^+$-A	0.847	0.015	11.537
$S_{Si}{}^+$-A to $S_{Si}{}^{2+}$	0.526	0.024	2.625

4. Conclusion

In summary, using first-principles methods, we have studied the defect configurations and the transition energy levels for S_{Si} substitution defects with different charged states. Besides the defect configuration with high symmetry, we discovered a new distortive structure for S_{Si}^{+}, which does not appear in previous PW91 or our PBE calculations. For S_{Si}^{+}, the symmetric structure (S_{Si}^{+}-A) and distortive structure (S_{Si}^{+}-B), which have almost the same energy, are separated by a 0.01 eV energy barrier. The calculated transition energy levels $\varepsilon(0/+)$ and $\varepsilon(+/2+)$ are both consistent with the experimental values. Moreover, we obtained the hole-capture cross sections for both a neutral and a +1 charged state. The hole-capture cross section for S_{Si}^{+} to S_{Si}^{2+} through S_{Si}^{+}-B agrees with our experiment, but the S_{Si}^{0} to S_{Si}^{+} process shows a much lower cross section because it is an Auger process. Hole capture through S_{Si}^{+}-A has negligibly low cross sections, so it has a low possibility of getting involved in the hole-capture process. Our calculations provide not only a deeper understanding of the defect properties of the S_{Si} substitution, but also a benchmark for the computational study of the carrier capture cross section using multi-phonon nonradiative recombination theory.

Data availability statement

The data that support the findings of this study are available upon reasonable request from the authors.

Acknowledgments

This work was supported by the National Natural Science Foundation of China (NSFC) under Grant Nos. 61722402 and 91833302, Shanghai Academic/Technology Research Leader (19XD1421300), the Program for Professor of Special Appointment (Eastern Scholar) (TP2019019), Fok Ying Tung Education Foundation (161060), and the Fundamental Research Funds for the Central Universities.

ORCID iDs

Yu-Ning Wu https://orcid.org/0000-0003-3970-3160
Shiyou Chen https://orcid.org/0000-0002-4039-8549

References

[1] Carey J E, Crouch C H, Shen M and Mazur E 2005 *Opt. Lett.* **30** 1773–5
[2] Li C-H, Zhao J-H, Yu X-Y, Chen Q-D, Feng J, Han P-D and Sun H-B 2017 *IEEE Sens. J.* **17** 2367–71
[3] Azzouzi G and Tazibt W 2013 *Energy Proc.* **41** 40–9
[4] Kim T G, Warrender J M and Aziz M J 2006 *Appl. Phys. Lett.* **88** 241902
[5] Jiang H and Chen C 2015 *J. Phys. Chem.* A **119** 3753–61
[6] Hall R N 1952 *Phys. Rev.* **87** 387
[7] Shockley W and Read W T 1952 *Phys. Rev.* **87** 835–42
[8] Wang J, Li W and Yin W-J 2020 *Adv. Mater.* **32** 1906115
[9] Carlson R O, Hall R N and Pell E M 1959 *J. Phys. Chem. Solids* **8** 81–3
[10] Krag W E and Zeiger H J 1962 *Phys. Rev. Lett.* **8** 485–7
[11] Engström O and Grimmeiss H G 1976 *J. Appl. Phys.* **47** 4090–7
[12] Grimmeiss H G, Janzén E and Skarstam B 1980 *J. Appl. Phys.* **51** 4212–17
[13] Brotherton S D, King M J and Parker G J 1981 *J. Appl. Phys.* **52** 4649–58
[14] Sclar N 1981 *J. Appl. Phys.* **52** 5207–17
[15] Janzén E, Stedman R, Grossmann G and Grimmeiss H G 1984 *Phys. Rev.* B **29** 1907–18
[16] Zeiger H J and kleiner W H 1985 *Mater. Res. Soc.* **46** 519–24
[17] Kleverman M, Grimmeiss H G, Litwin A and Janzén E 1985 *Phys. Rev.* B **31** 3659–66
[18] Krag W E, Kleiner W H and Zeiger H J 1986 *Phys. Rev.* B **33** 8304–20
[19] Astrov Y A, Portsel L M, Lodygin A N and Shuman V B 2011 *Semicond. Sci. Technol.* **26** 055021
[20] Guenther K-M, Gimpel T, Tomm J W, Winter S, Ruibys A, Kontermann S and Schade W 2014 *Appl. Phys. Lett.* **104** 042107
[21] Gwozdz K, Kolkovsky V, Weber J, Yakovleva A A and Astrov Y A 2019 *Phys. Status Solidi* a **216** 1900303
[22] Mo Y, Bazant M Z and Kaxiras E 2004 *Phys. Rev.* B **70** 205210
[23] Coutinho J, Torres V J B, Jones R and Briddon P R 2003 *Phys. Rev.* B **67** 035205
[24] Huang K and Rhys A 1950 *Proc. R. Soc.* A **204** 406–23
[25] Freed K F and Jortner J 1970 *J. Chem. Phys.* **52** 6272–91
[26] Henry C H and Lang D V 1977 *Phys. Rev.* B **15** 989–1016
[27] Kubo R and Toyozawa Y 1955 *Prog. Theor. Phys.* **13** 160
[28] Lax M 1952 *J. Chem. Phys.* **20** 1752–60
[29] Shi L and Wang L-W 2012 *Phys. Rev. Lett.* **109** 245501
[30] Shi L, Xu K and Wang L-W 2015 *Phys. Rev.* B **91** 205315
[31] Alkauskas A, Yan Q M and Van De Walle C G 2014 *Phys. Rev.* B **90** 075202
[32] Alkauskas A, McCluskey M D and Van De Walle C G 2016 *J. Appl. Phys.* **119** 181101
[33] Xiao Y, Wang Z, Shi L, Jiang X, Li S and Wang L 2020 *Sci. China* **63** 277312
[34] Yang J-H, Shi L, Wang L-W and Wei S-H 2016 *Sci. Rep.* **6** 21712
[35] Li J Q, Yuan Z K, Chen S Y, Gong X G and Wei S H 2019 *Chem. Mater.* **31** 826–33
[36] Kim S, Park J-S, Hood S N and Walsh A 2019 *J. Mater. Chem.* A **7** 2686–93
[37] Chen Z, Zhang P-Z, Zhou Y, Zhang X, Liu X, Hou Z, Tang J and Li W 2020 *J. Phys. Chem. Lett.* **11** 10354–61
[38] Xu Y, Yang J-H, Chen S and Gong X-G 2021 *Phys. Rev. Mater.* **47** 025403
[39] Barmparis G D, Puzyrev Y S, Zhang X-G and Pantelides S T 2015 *Phys. Rev.* B **92** 214111
[40] Li J, Zhu H-F, Zhang Y-Y, Yuan Z-K, Chen S and Gong X-G 2017 *Phys. Rev.* B **96** 104103
[41] Hohenberg P and Kohn W 1964 *Phys. Rev.* **136** B864–B71
[42] Kohn W and Sham L J 1965 *Phys. Rev.* **140** A1133–A8
[43] Kresse G and Furthmuller J 1996 *Comput. Mater. Sci.* **6** 15–50
[44] Kresse G and Furthmuller J 1996 *Phys. Rev.* B **54** 11169–86
[45] Blöchl P E 1994 *Phys. Rev.* B **50** 17953–79
[46] Heyd J, Scuseria G E and Ernzerhof M 2003 *J. Chem. Phys.* **118** 8207–15
[47] Wei S-H 2004 *Comput. Mater. Sci.* **30** 337–48
[48] Zhang S B, Wei S-H, Zunger A and Katayama-Yoshida H 1998 *Phys. Rev.* B **57** 9642–56
[49] Lany S and Zunger A 2008 *Phys. Rev.* B **78** 235104

[50] Perdew J P, Burke K and Ernzerhof M 1996 *Phys. Rev. Lett.* **77** 3865–8
[51] Giannozzi P *et al* 2009 *J. Phys.: Condens. Matter* **21** 395502
[52] Giannozzi P, De Angelis F and Car R 2004 *J. Chem. Phys.* **120** 5903–15
[53] Pässler R 1974 *Czech. J. Phys.* B **26** 322–39
[54] Pässler R 1982 *Czech. J. Phys.* B **32** 846–83
[55] Pässler R 1976 *Phys. Status Solidi* b **78** 625–35
[56] Landsberg P T 2009 Recombination in Semiconductors (Cambridge: Cambridge University Press) (https://doi.org/10.1017/CBO9780511470769)
[57] Lyons J L, Janotti A and Van de Walle C G 2012 *Phys. Rev. Lett.* **108** 156403
[58] Henkelman G, Uberuaga B P and Jónsson H 2000 *J. Chem. Phys.* **113** 9901–4
[59] Bemski G 1958 *Phys. Rev.* **111** 1515–18
[60] Huang K 1981 *Contemp. Phys.* **22** 599